



**HAL**  
open science

# Direct band gap In<sub>x</sub>Ga<sub>1-x</sub>As/Ge type II strained quantum wells for short-wave infrared p-i-n photodetector

N. Harbi, N. Sfina, A. Jbeli, J.-L. Lazzari, M. Said

► **To cite this version:**

N. Harbi, N. Sfina, A. Jbeli, J.-L. Lazzari, M. Said. Direct band gap In<sub>x</sub>Ga<sub>1-x</sub>As/Ge type II strained quantum wells for short-wave infrared p-i-n photodetector. *Optical Materials*, 2015, 46, pp.472-480. 10.1016/j.optmat.2015.05.006 . hal-03144491

**HAL Id: hal-03144491**

**<https://hal.science/hal-03144491>**

Submitted on 17 Feb 2021

**HAL** is a multi-disciplinary open access archive for the deposit and dissemination of scientific research documents, whether they are published or not. The documents may come from teaching and research institutions in France or abroad, or from public or private research centers.

L'archive ouverte pluridisciplinaire **HAL**, est destinée au dépôt et à la diffusion de documents scientifiques de niveau recherche, publiés ou non, émanant des établissements d'enseignement et de recherche français ou étrangers, des laboratoires publics ou privés.

# Direct band gap $\text{In}_x\text{Ga}_{1-x}\text{As}/\text{Ge}$ type II strained quantum wells for short-wave infrared p-i-n photodetector

N. Harbi, N. Sfina, A. Jbeli, J.-L. Lazzari, M. Said

► **To cite this version:**

N. Harbi, N. Sfina, A. Jbeli, J.-L. Lazzari, M. Said. Direct band gap  $\text{In}_x\text{Ga}_{1-x}\text{As}/\text{Ge}$  type II strained quantum wells for short-wave infrared p-i-n photodetector. *Optical Materials*, Elsevier, 2015, 46, pp.472-480. 10.1016/j.optmat.2015.05.006 . hal-03144491

**HAL Id: hal-03144491**

**<https://hal.archives-ouvertes.fr/hal-03144491>**

Submitted on 17 Feb 2021

**HAL** is a multi-disciplinary open access archive for the deposit and dissemination of scientific research documents, whether they are published or not. The documents may come from teaching and research institutions in France or abroad, or from public or private research centers.

L'archive ouverte pluridisciplinaire **HAL**, est destinée au dépôt et à la diffusion de documents scientifiques de niveau recherche, publiés ou non, émanant des établissements d'enseignement et de recherche français ou étrangers, des laboratoires publics ou privés.

# Direct band gap $\text{In}_x\text{Ga}_{1-x}\text{As}/\text{Ge}$ type II strained quantum wells for short-wave infrared p-i-n photodetector

N. Harbi<sup>a</sup>, N. Sfina<sup>a,c,\*</sup>, A. Jbeli<sup>a,d</sup>, J.-L. Lazzari<sup>b</sup>, M. Said<sup>a</sup>

<sup>a</sup> Laboratoire de la Matière Condensée et des Nanosciences (LMCN), Département de Physique, Faculté des Sciences de Monastir, Avenue de l'Environnement, 5019 Monastir, Tunisia

<sup>b</sup> Centre Interdisciplinaire de Nanoscience de Marseille (CINaM), UMR CNRS 7325, Aix-Marseille Université, Case 913, Campus de Luminy, 13288 Marseille Cedex 9, France

<sup>c</sup> Faculty of Science and Art, King Khalid University (KKU), Mahail Assir, Saudi Arabia

<sup>d</sup> College of Sciences & Humanities of Ghat, Majmaah University, P.O. Box 445, Ghat 11914, Saudi Arabia

## ARTICLE INFO

### Article history:

Received 1 March 2015

Received in revised form 21 April 2015

Accepted 10 May 2015

Available online xxxxx

### Keywords:

Band engineering

Absorption

Strained  $\text{Ge}/\text{In}_x\text{Ga}_{1-x}\text{As}$

Infrared photodetector

Dark current

## ABSTRACT

We theoretically investigate  $\text{GaAs}/\text{Ge}/\text{InGaAs}$  as a quantum wells for the design of short-wave infrared p-i-n photodetectors in which the quantum well  $\text{Ge}/\text{InGaAs}$  is the active region. At room temperature, strained  $\text{Ge}/\text{In}_x\text{Ga}_{1-x}\text{As}$  becomes a direct band gap when In composition  $x$  is lower than 2.5% and 5% respectively. We have calculated the electronic band parameters for the heterointerface  $\text{Ge}/\text{In}_x\text{Ga}_{1-x}\text{As}$ . Then, a type-II strain  $\text{GaAs}/\text{Ge}/\text{In}_{0.35}\text{Ga}_{0.65}\text{As}/\text{GaAs}$  quantum wells heterostructure optimized in terms of compositions and thicknesses is studied by solving Schrödinger equation as well as the absorption coefficient ( $>1.5 \times 10^4 \text{ cm}^{-1}$ ). These computations have been used for the study of p-i-n infrared photodetectors operating at room temperature in the range 1.3–1.55  $\mu\text{m}$ . The electron transport in the  $\text{GaAs}/\text{Ge}/\text{In}_{0.35}\text{Ga}_{0.65}\text{As}/\text{GaAs}$  multi-quantum wells-based p-i-n structure was analyzed and numerically simulated taking into account tunneling process and thermally activated transfer through the barriers mainly. The temperature dependence of dark current mechanisms and zero-bias resistance area product ( $R_0A$ ) have been analyzed. Extracted from current-voltage characteristics,  $R_0A$  products above  $3.6 \cdot 10^6 \Omega \text{ cm}^2$  at 77 K were calculated, and the quantitative analysis of the  $J$ - $V$  curves showed that the dark current density of  $\text{Ge}/\text{In}_{0.35}\text{Ga}_{0.65}\text{As}$  photodetector is dominated by generation-recombination processes. The suitability of the modeled photodetector is approved by its feasibility of achieving good device performance near room temperature operating at 1.55  $\mu\text{m}$ . Quantum efficiency of  $\sim 90\%$  and responsivity  $\sim 0.6 \text{ A/W}$ , have been achieved.

## 1. Introduction

High-electron mobility materials such as  $\text{In}_x\text{Ga}_{1-x}\text{As}$  have been advantageously used for decades through band gap engineering in various applications ranging from high-power, high-frequency electronics to optoelectronics [1,2]. Many results highlighted the significant challenges faced by epi, process technologists to achieve a successful combination of Ge and III-V materials on Si substrate [3,4]. The  $\text{Ge}/\text{GaAs}$  heterostructure was one of the first discovered pairs of the semiconductors having nearly equal lattice constants and different band gaps [5]. Despite the equality of Ge and GaAs lattice constants, there are several difficulties of growth of GaAs at Ge due to the antiphase domains, which lead to the formation radiative and nonradiative recombination centers as a result of

the effect of residual co-doping [6]. Nevertheless, recently, some technologies for growing are found to eliminate these effects [7,8]. With the ability to synthesize highly strained layers of Ge, we can further investigate optical and transport properties [9]. These technologies have resulted in development of  $\text{Ge}/\text{GaAs}$  multi-quantum-well near infrared and laser structures as well as efficient photovoltaic structures on the Ge substrates [10,11]. Thus,  $\text{Ge}/\text{GaAs}$  heterojunctions have been appropriate for optoelectronic applications due to the progress in the growth techniques. However, GaAs based heterostructures with Ge and  $\text{Ge}/\text{InGaAs}$  quantum wells are grown by laser assisted sputtering, for the development of light emitting devices operating at wavelengths close to 1.5  $\mu\text{m}$  [12]. In Germanium the top of the valence band is located in the  $\Gamma$ -point and the lower valley in the conduction band is the L-valley. The difference between the edges of the L- and  $\Gamma$ -valleys in the conduction band is only 136 meV [13], whereas the energy of direct optical transitions at room temperature corresponds to the wavelength 1.55  $\mu\text{m}$ . The GaAs-based

\* Corresponding author at: Laboratoire de la Matière Condensée et des Nanosciences (LMCN), Département de Physique, Faculté des Sciences de Monastir, Avenue de l'Environnement, 5019 Monastir, Tunisia.

E-mail address: sfina\_fsm@yahoo.fr (N. Sfina).

structures with Ge and combined Ge/InGaAs quantum wells have been proven to be another promising material for the infrared photodetector covering all telecommunication windows because the bandgap of InGaAs can be tuned by adjusting In concentrations. In a structure with Ge and  $\text{In}_x\text{Ga}_{1-x}\text{As}$  layers the layer thicknesses and the In content can be chosen such that the conduction band bottom in the combined quantum well will be in the  $\Gamma$ -valley of  $\text{In}_x\text{Ga}_{1-x}\text{As}$  and the valence band top will be in the Ge layer. The energy of the electron transitions from the  $\text{In}_x\text{Ga}_{1-x}\text{As}$  conduction band to the Ge valence band in such quantum wells will be in the 1.3–1.55  $\mu\text{m}$  wavelength range. These transitions are direct in the momentum space, but indirect in the coordinate space. Due to a small electron mass in the  $\Gamma$ -valley of Ge [14] and a small value of band offset of the  $\Gamma$ -valley in the Ge/ $\text{In}_x\text{Ga}_{1-x}\text{As}$  heterojunction, the electrons of the lower subband bottom in the conduction band deeply penetrate in the Ge layer, causing a fairly large overlap of the conduction and valence band wave functions.

The main objective of this paper is the theoretical simulation of GaAs/Ge/ $\text{In}_{0.35}\text{Ga}_{0.65}\text{As}$ /GaAs p–i–n infrared photodetectors operating at room temperature around 1.3–1.55  $\mu\text{m}$ . The active layer of the infrared photodetector consists of alternating layers of Ge/ $\text{In}_{0.35}\text{Ga}_{0.65}\text{As}$  MQWs (Multi Quantum Wells) grown on relaxed GaAs substrates. The active photodetector absorption layer consists of 5 periods Ge/ $\text{In}_{0.35}\text{Ga}_{0.65}\text{As}$  quantum wells separated by 5-nm-thick GaAs spacers. In order to design such device, it is very important to determine the electronic properties of strained Ge/ $\text{Ga}_{1-x}\text{In}_x\text{As}$ , such as band gap energy and bands discontinuities as a function of composition. In a first step toward the calculation of optical properties of Ge/ $\text{Ga}_{1-x}\text{In}_x\text{As}$  quantum-well, we report the band offsets at Ge/ $\text{Ga}_{1-x}\text{In}_x\text{As}$  strained/ (001)-oriented relaxed interfaces as well as the absorption coefficient spectrum at room temperature. Then, we investigate the dark current contributing mechanisms through the temperature dependence. The dark current versus the bias voltage, the zero-bias resistance area product ( $R_0A$ ), quantum efficiency and responsivity are finally presented and discussed.

## 2. Calculation of material parameters

In order to perform a simulation of the optoelectronics characteristics of Ge/ $\text{In}_x\text{Ga}_{1-x}\text{As}$  near-infrared photodetector, material parameters of Ge and  $\text{Ga}_{1-x}\text{In}_x\text{As}$  such as band offsets for the conduction and valence band at  $\Gamma$  ( $\Delta E_{c,\Gamma}$ ), L ( $\Delta E_{c,L}$ ), heavy and light holes ( $\Delta E_{v,hh}$ ), ( $\Delta E_{v,lh}$ ) and effective masses of electrons and holes, are needed. Using the parameters listed in Table 1. These data

**Table 1**  
Material parameters used in the calculations are extracted from [14]. The definition of these different parameters is as in.

Parameters	Ge	InAs	GaAs
$a$ (Å)	5.656	6.0583	5.654
$m_{c,\Gamma}$ ( $m_0$ )	0.038	0.023	0.0636
$m_{t,L}$ ( $m_0$ )	0.0815	0.05	0.075
$m_{l,L}$ ( $m_0$ )	1.59	0.64	1.9
$m_{v,hh}$ ( $m_0$ )	0.044	0.39	0.41
$m_{v,lh}$ ( $m_0$ )	0.284	0.11	0.071
$E_{g,\Gamma}$ (eV)	0.802	0.269	1.424
$E_{g,L}$ (eV)	0.661	1.895	1.714
$A$ (eV)	0.289	0.381	0.341
$a_c$ (eV)	-5.16	-5.08	-7.17
$a_v$ (eV)	-3.1	-1	-1.16
$\gamma_1$	13.38	0.634	1.866
$\gamma_2$	4.24	-1.38	0.391
$b$ (eV)	-2.08	-1.8	-1.7
$c_{11}$ (GPa)	128.5	832.9	1188
$c_{12}$ (GPa)	48.3	452.6	538
$E_{v,av}$ (eV)	0	-6.67	-6.92

enable one to calculate the band offsets, the conduction and valence-band discontinuities between the Ge strained layer and the  $\text{In}_x\text{Ga}_{1-x}\text{As}$  substrate. With this aim, we have adopted the procedure outlined in Ref. [15], we have calculated the conduction and valence-band discontinuities for strained Ge/ $\text{Ga}_{1-x}\text{In}_x\text{As}$  in minimums  $\Gamma$ , L, hh and lh as a function of  $x$  compositions. The conduction and valence-band discontinuities between the Ge strained layer and the (001)-oriented relaxed  $\text{In}_x\text{Ga}_{1-x}\text{As}$  substrate are

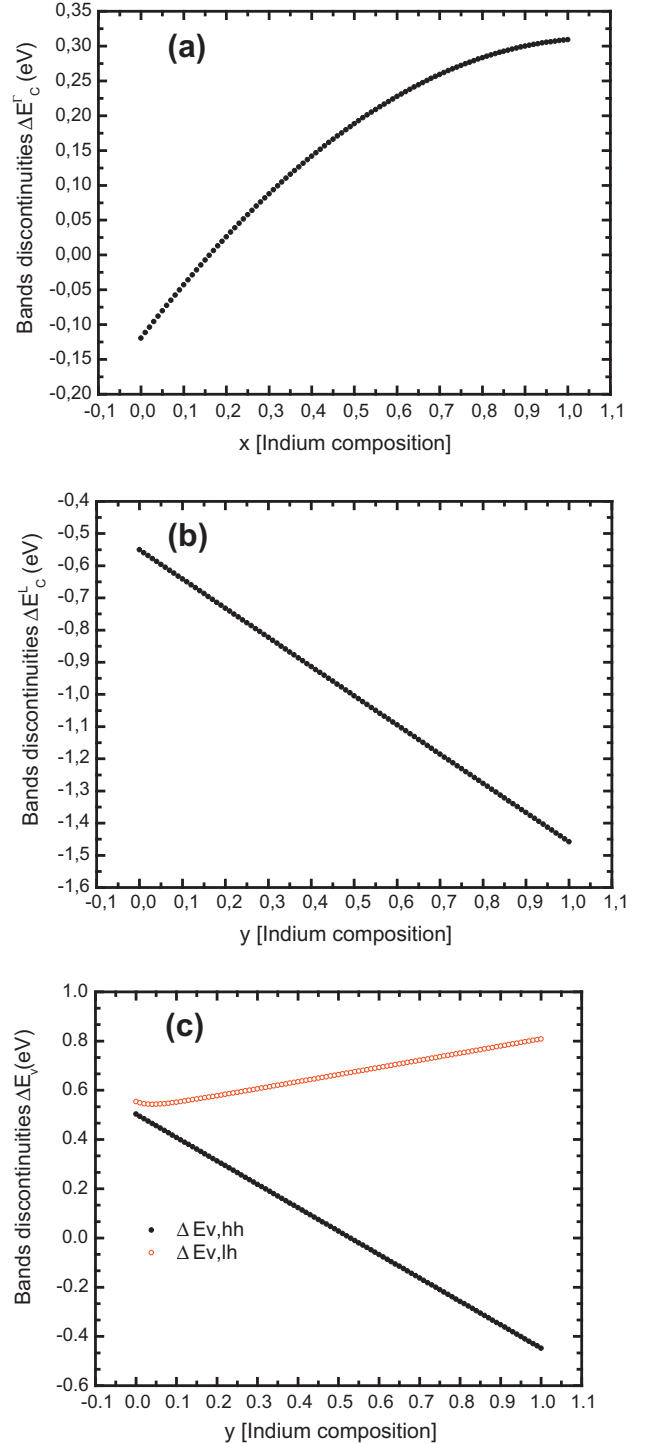


**Fig. 1.** (a) Conduction-band offsets  $\Delta E_c^\Gamma$  in minimum  $\Gamma$ , (b) conduction-band offsets  $\Delta E_c^L$  in minimum L and (c) valence-band discontinuities  $\Delta E_v^{hh}$ ,  $\Delta E_v^{lh}$  of heavy and light holes at Ge/ $\text{Ga}_{1-x}\text{In}_x\text{As}$  heterointerface.

plotted in Fig. 1. Fig. 1(a) and (b) shows the conduction band offsets at  $\Gamma$  and L points, respectively. Fig. 1(c) shows the valence band offsets for heavy and light holes. The approximate analytical expression for the conduction and valence-band discontinuity of a strained Ge on a relaxed  $\text{In}_x\text{Ga}_{1-x}\text{As}$  substrate, presented in Eqs. (1)–(4):

$$\Delta E_C^\Gamma(x) = -0.11951 + 0.80357x - 0.37498x^2 \quad (1)$$

$$\Delta E_C^L(x) = -0.55051 - 0.9074x - 1.70491 \cdot 10^{-5}x^2 \quad (2)$$

$$\Delta E_V^{hh}(x) = 0.50339 - 0.95151x + 1.78887 \cdot 10^{-5}x^2 \quad (3)$$

$$\Delta E_V^{lh}(x) = 0.53141 + 0.24296x + 0.03762x^2 \quad (4)$$

The band gap energy of  $\text{In}_x\text{Ga}_{1-x}\text{As}$  is linearly interpolated between the value of bulk GaAs and InAs. The analytical expressions find with EPM calculation [16] are quoted as follows

$$E_g^{(\Gamma)}(x) = 1.42 - 1.05724x - 0.0018x^2 \quad (5)$$

$$E_g^{(L)}(x) = 1.73 - 0.66x \quad (6)$$

$$E_g^{(X)}(x) = 1.91 - 0.54x \quad (7)$$

Fig. 2 shows the calculated relaxed and strained band-gap energies ( $E_g^\Gamma$ ;  $E_g^L$ ;  $E_g^{\Gamma-hh}$ ;  $E_g^{\Gamma-lh}$ ;  $E_g^{L-hh}$  and  $E_g^{L-lh}$ ) versus composition  $x$  of indium content in  $\text{In}_x\text{Ga}_{1-x}\text{As}$ . The calculated strained band-gap energies versus composition  $x$  for Ge strained layer and the  $\text{In}_x\text{Ga}_{1-x}\text{As}$  substrate are also plotted. The Ge/ $\text{In}_x\text{Ga}_{1-x}\text{As}$  (001) alloy may have an indirect strained band gap at In-fractions higher than 2.5% for ( $E_g^{\Gamma-hh}$ ,  $E_g^{\Gamma-lh}$ ) and 5% for ( $E_g^{\Gamma-hh}$ ,  $E_g^{L-hh}$ ) at room temperatures. Regarding the Ge/ $\text{In}_x\text{Ga}_{1-x}\text{As}$ , the direct-to-indirect crossover may occur at a In-fraction of 2.5% and 5% for  $\Gamma$ ,  $L$ - $hh$  and  $\Gamma$ ,  $L$ - $lh$  respectively at 300 K. latter values are consistent with the experimental results pointed out by recent investigations of Ref. [17] our theoretically determined values are plotted in Fig. 2(a). The analytical expressions are quoted as follows:

$$E_g^{\Gamma-hh}(x) = 0.79671 + 0.54924x - 0.37679x^2 \quad (8)$$

$$E_g^{\Gamma-lh}(x) = 0.76185 - 0.18745x - 0.4229x^2 \quad (9)$$

$$E_g^{L-hh}(x) = 0.8177 - 0.00251x - 1.37129 \cdot 10^{-5}x^2 \quad (10)$$

$$E_g^{L-lh}(x) = 0.78285 - 0.73919x - 0.04612x^2 \quad (11)$$

with energies given in eV. As one can see, the strained band gap energies could be linearly interpolated between the values of GaAs and InAs, as well. The L point is only subject to hydrostatic shifts. Therefore both the minima  $\Gamma$ - $lh$  and  $L$ - $lh$  strained band gaps are lower than the relaxed one. At the contrary, due to the sign of the uniaxial component,  $\Gamma$ - $lh$  and  $L$ - $lh$  strained gaps are decreased under the stress effect. The  $\Gamma$ - $hh$  and  $L$ - $hh$  strained gaps increased, in respect to the relaxed gaps.

### 3. Modeling of Ge/InGaAs QW

The investigated GaAs/Ge/ $\text{In}_x\text{Ga}_{1-x}\text{As}$ /GaAs heterostructure consists of Ge/ $\text{In}_x\text{Ga}_{1-x}\text{As}$  combined quantum well. Further, we will assume  $x = 0.35$  because this value is close to maximum for such quantum wells. It is readily seen that the  $\Gamma$ -valley bottom of  $\text{In}_{0.35}\text{Ga}_{0.65}\text{As}$  lies about 40 meV lower than that in Ge, and the  $L$ -valley bottom in  $\text{In}_{0.35}\text{Ga}_{0.65}\text{As}$  is by 65 meV higher than in GaAs. So it is clear that for relatively narrow Ge layers the lowest

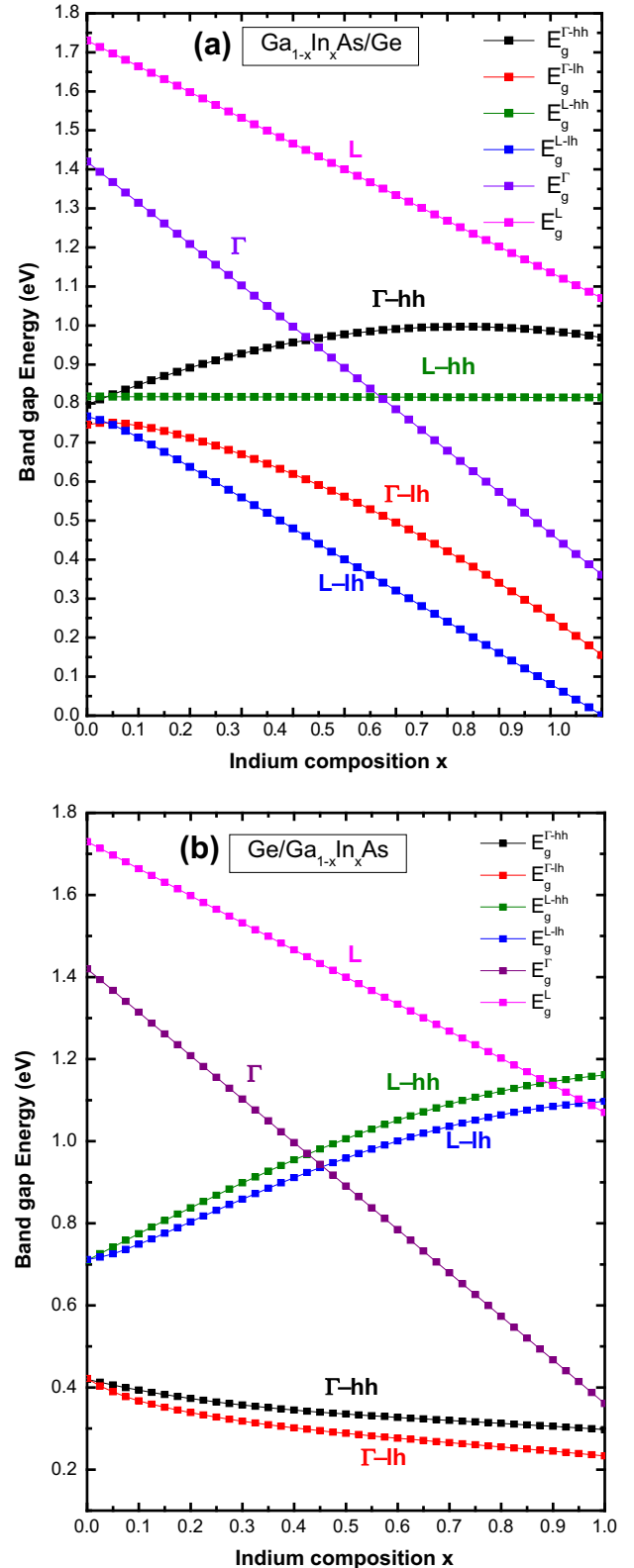
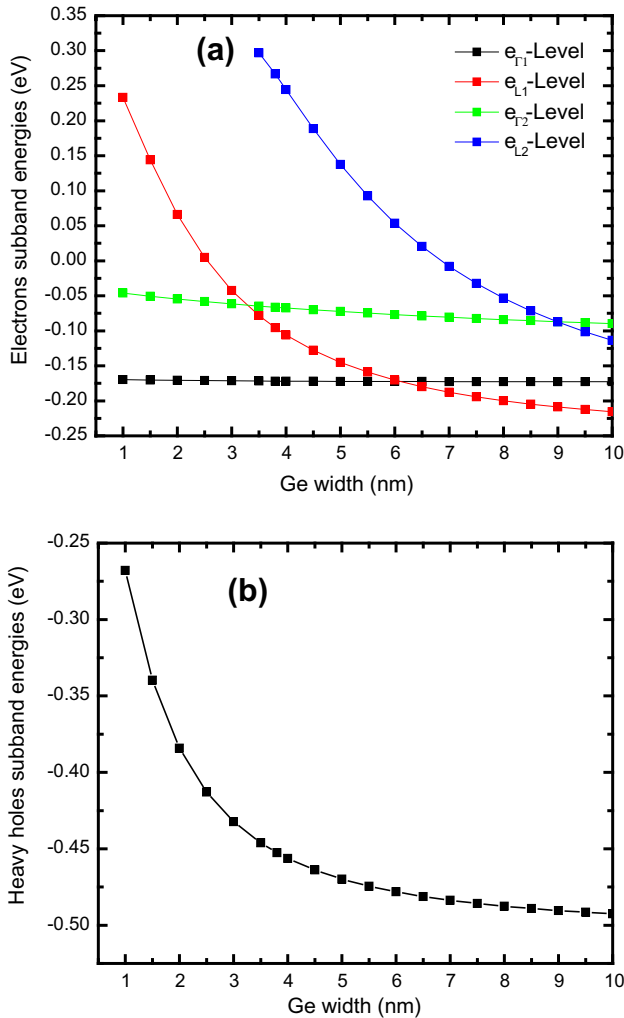


Fig. 2. Evolution of relaxed and strained band gap energies at room temperature as a function of indium content, in (a) strained Ge layer on relaxed  $\text{In}_x\text{Ga}_{1-x}\text{As}$  substrate, and (b) strained  $\text{In}_x\text{Ga}_{1-x}\text{As}$  layer on relaxed Ge substrate, respectively at  $\Gamma$ - and  $L$ -valleys respectively.

level of the conduction band is the  $\Gamma$ -valley level with the wave function maximum in the  $\text{In}_{0.35}\text{Ga}_{0.65}\text{As}$  layer. The wave function maximum of the ground hole level is located in the Ge layer. The

energy levels of these subbands can be calculated by solving the one-dimensional Schrödinger equation following the envelope function approximation [18]. The energies of the different subband edges are plotted in Fig. 3. The plot presents that the quantum confinement energies increase with reducing the Ge layer width. As seen from Fig. 3(a), for the Ge layer thickness values less than 3.8 nm the lowest energy levels are the  $\Gamma$ -levels. The energy of the lowest level in the  $\Gamma$ -valley is practically independent of the Ge layer width. The reason for this is that the wave function of this state is localized in the  $\text{In}_{0.35}\text{Ga}_{0.65}\text{As}$  layer mainly. For the Ge layer thickness values less than 3.8 nm, the energy levels decrease until Ge layer thickness 3.8 nm for heavy holes and for electrons at L-point and then become stationary. In Fig. 4 we have illustrates the position of the detection energy in a quantum well for the hh, L and  $\Gamma$ -valleys of GaAs/Ge/ $\text{In}_{0.35}\text{Ga}_{0.65}\text{As}$ /GaAs heterostructure, depending on Ge layer thickness. The thickness of the  $\text{In}_{0.35}\text{Ga}_{0.65}\text{As}$  quantum well is 8 nm (which is close to the critical value). Note that a laser with an 8-nm-wide  $\text{In}_{0.35}\text{Ga}_{0.65}\text{As}$  quantum well in GaAs generates light at the wavelength of 1.13  $\mu\text{m}$  at room temperature [19]. As seen from Fig. 4, the interband transitions correspond to the wavelengths in the 1.55  $\mu\text{m}$  range. As the Ge layer is a deeper quantum well for the holes than the  $\text{In}_{0.35}\text{Ga}_{0.65}\text{As}$  layer, the wave function of the holes ground state is situated in the Ge layer mainly (see Fig. 5). So, the transitions in such heterostructures are indirect in the



**Fig. 3.** (a) Electron confinement-energies levels in  $\Gamma$  and L-valley. (b) Heavy hole confinement-energies for the GaAs/Ge/ $\text{In}_{0.35}\text{Ga}_{0.65}\text{As}$ /GaAs heterostructure as a function of Ge layer thickness.

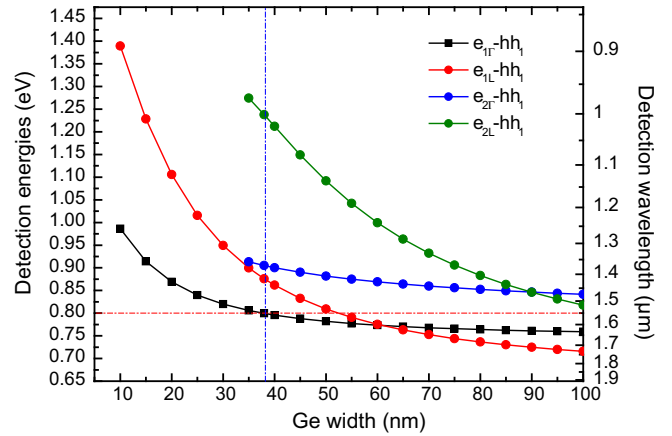


**Fig. 4.** Room temperature evolution of the  $\Gamma$ - and L-valley energies and the wavelength of radiation corresponding to the edge of direct-band transitions of  $hh_1-e_{\Gamma_n}$ , and  $hh_1-e_{L_n}$  ( $n = 1$  and  $n = 2$ ) transitions versus the Ge layer thickness in GaAs/Ge/ $\text{In}_{0.35}\text{Ga}_{0.65}\text{As}$ /GaAs heterostructure.

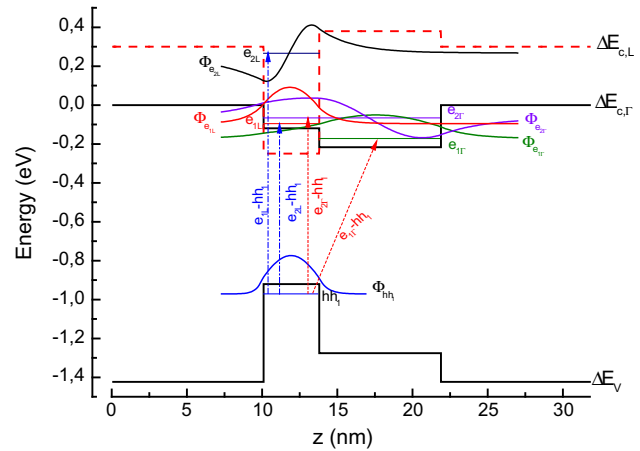


**Fig. 5.** Conduction and valence band-edges minima for the GaAs/Ge/ $\text{In}_{0.35}\text{Ga}_{0.65}\text{As}$ /GaAs heterostructure. For each heterostructure  $e_{\Gamma_n}$ ,  $e_{L_n}$ , and  $hh_1$  quantum levels are drawn with their relative wave functions. The heterostructure stack is optimally designed for an while the  $e_{\Gamma_1}$ - $hh_1$ ,  $e_{L_1}$ - $hh_1$ ,  $e_{L_1}$ - $hh_1$  and  $e_{L_2}$ - $hh_1$  transition gaps are 0.8 eV, 0.905 eV, 0.875 eV and 1.238 eV, respectively.

coordinate space. Fig. 5 shows the conduction and valence band-edges minima for the GaAs/Ge/ $\text{In}_{0.35}\text{Ga}_{0.65}\text{As}$ /GaAs heterostructure. For each heterostructure  $e_{\Gamma_n}$ ,  $e_{L_n}$ , and  $hh_1$  quantum levels are drawn with their relative wave functions. The heterostructure stack is optimally designed for an while the  $e_{\Gamma_1}$ - $hh_1$ ,  $e_{L_1}$ - $hh_1$ ,  $e_{L_1}$ - $hh_1$  and  $e_{L_2}$ - $hh_1$  transition gaps are 0.8 eV, 0.905 eV, 0.875 eV and 1.238 eV, respectively. The thickness of Ge and  $\text{In}_{0.35}\text{Ga}_{0.65}\text{As}$  layers is 3.8 and 8 nm, respectively.

Next, we calculated the absorption coefficient in QW structures with the following theoretical method. The theoretical dispersions of the absorption coefficient are obtained from the imaginary and real parts of the estimated dielectric constant, respectively. In the estimation of the free-carrier contribution, energy-and polarization-dependent momentum matrix elements [15] and line broadening represented by a Gaussian line shape function were taken into account. The contributions of free-carrier-transitions to the imaginary part is given by:

$$\alpha(\hbar\omega) = \frac{e^2}{\epsilon_0 m_0^2 L_{\text{eff}}} \frac{m_{eh}}{\Pi \hbar^2} \sum_i \sum_j |M_{ij}|^2 \left| \int \Psi_{ei}(z) \Psi_{hj}(z) dz \right|^2 \times \int M(E) F(E + E_g + E_{ei} + E_{hj} - \hbar\omega) dE \quad (12)$$

where  $L_{eff}$  is the thickness of the QW,  $m_{eh}$  is the reduced hole effective mass  $E_g$ ,  $E_{ei}$  and  $E_{hj}$  are the energy gap, and the quantized energies of the  $n = i$  electron and  $n = j$  hole, respectively, and  $\hbar\omega$  denotes the photon energy. The energies  $E_{ei}$  and  $E_{hj}$ , and their related wave functions  $\Psi_{ei}(z)$  and  $\Psi_{hj}(z)$ , respectively, are solutions of the one-dimensional Schrödinger equations. The quantity  $|M_b|^2$  is the average matrix element for the Bloch state.

To achieve the absorption coefficient due to electronic transitions inter conduction and valence bands, given by Eq. (12), one needs to know the band structures and the corresponding wave functions. The one-dimensional Schrödinger equation following the envelope function approximation [19] is useful technique for analyzing the conduction and the valence band structures near the band edges. Fig. 6 illustrated the absorption coefficient calculated using this model at 300 K. The absorption spectrum shows the typical staircase line shape proportional to the joint density of states in direct transition in Ge/In<sub>0.35</sub>Ga<sub>0.65</sub>As QW. In fact, as demonstrated in Ref. [20], the near-edge absorption spectrum of Ge/InGaAs QWs is dominated by transitions involving heavy hole and light hole valence band states and conduction band states at the  $\Gamma$  point, spatially confined by a type II profile. In the same spatial region, L point conduction band states are also present. They have top energy with respect to the conduction band states at  $\Gamma$ . Nevertheless, the role of L states in the near-edge absorption region can be considered due to the important oscillator strength related to the  $k$ -indirect nature of the  $\Gamma$ -L transitions. In the same spatial region, L point conduction band states are also present. They have high energy compared to the conduction band states at  $\Gamma$ . In this simple model, the quantization energy, the wave function, and the matrix element were calculated at various Ge well widths. The matrix elements are proportional to the square of overlap integral between electron and holes wave function. However, the role of L states in the near-edge absorption region can be taken account due to the important oscillator strength related to the  $k$ -indirect nature of the  $\Gamma$ -L transitions. Next, for the chosen set of near-edge states, we have calculated the out-of-plane wave function oscillator strength of the  $e$ -hh and  $e$ -lh transitions. The fundamental  $e_{\Gamma 1-hh_1}$ ,  $e_{\Gamma 2-hh_1}$ ,  $e_{L1-hh_1}$  and  $e_{L2-hh_1}$  transitions, which is defined by the expression:

$$f_{i-f} = \frac{2m_0}{\hbar^2} (E_i - E_f) |\langle \Psi_i | z | \Psi_f \rangle|^2 \quad (13)$$

where  $m_0$  is the free electron mass,  $\hbar$  is the Planck constant,  $|\Psi_i\rangle$  and  $|\Psi_f\rangle$  are the initial and final states respectively,  $(E_i - E_f)$  is the energy difference between the two states and  $\langle \Psi_i | z | \Psi_f \rangle$  is the dipole matrix element of the fundamental transition (see [21] and reference therein). Fig. 7 shows the oscillator strengths versus the Ge quantum well thickness for normal incident radiation. In particular, the real direct transitions in the Ge region, at the  $\Gamma$  and L, point.

#### 4. p-i-n modeling and current simulation

The MQW-design structure under investigation consists of 5 periods of intrinsic Ge/In<sub>0.35</sub>Ga<sub>0.65</sub>As type II QWs separated by a GaAs barrier. The thick of Ge layer is 3.8 nm, and the thick of In<sub>0.35</sub>Ga<sub>0.65</sub>As layer is 8 nm. This active region consisting of 5 periods is embedded between 70 nm GaAs relaxed layers. These GaAs contacts are  $n$  and  $p$ -doped ( $N_A = N_D = 1 \times 10^{18} \text{ cm}^{-3}$ ). For the sake of simplicity, we assume that there are no impurities or defects in the host lattice. The ground state of this 2D system is described using the effective mass approximation [22]. The theoretical techniques and numerical methods used in this paper are based on the one dimensional Schrödinger equation for an electron within a heterostructure semiconductor. Since the charge distribution in the structure also modifies the quantum well potential we need

a self-consistent solution of Schrödinger's wave equation and Poisson's equation. Assuming a slowly varying effective mass, a Ben-Daniel-Duke Hamiltonian is used [23]:

$$-\frac{\hbar^2}{2m_0} \frac{d}{dz} \left( \frac{1}{m(z)} \frac{d}{dz} \right) + V_B(z) + V_H(z) + V_{xc}(z) + eFz \Psi_i(z) = E_i \Psi_i(z) \quad (14)$$

where  $V_B$ ,  $V_H$ ,  $V_{xc}$  and  $eFz$  are the quantum confined potential, the Hartree potential, the exchange correlation potential and the external potential term induced by the uniform applied electric field respectively. The Hartree potential is obtained from the Poisson equation as follows:

$$\epsilon_0 \frac{d}{dz} \left[ \epsilon_r(z) \frac{d}{dz} V_H(z) \right] = e^2 [N_D(z) - N_A(z) + p(z) - n(z)] \quad (15)$$

where  $\epsilon_r$  is the relative permittivity,  $e$  is the electron charge,  $p$  and  $n$  are free holes and electrons concentrations, and  $N_D$  and  $N_A$  the doping concentrations. After the discrete energy levels  $E_i$  and wave function  $\Psi_i$  are determined, the electron and hole densities in the QWs, assuming a 2D density of states, are given by [24]

$$n(z) = \frac{m_0^* kT}{\pi \hbar^2} \sum_{ie} \ln \left[ 1 + \exp \left( \frac{E_F - E_{ie}}{kT} \right) \right] |\Psi_{ie}(z)|^2 \quad (16)$$

$$p(z) = \frac{m_0^* kT}{\pi \hbar^2} \sum_{ihh} \ln \left[ 1 + \exp \left( \frac{E_F - E_{ihh}}{kT} \right) \right] |\Psi_{ihh}(z)|^2 \quad (17)$$

where  $E_{ie}$  and  $E_{ihh}$  are the  $i$ th eigenvalues for electrons and holes, respectively.  $E_F$  refers to the Fermi level which is determined by solving numerically the equation of charge neutrality. The Schrödinger equation is resolved both for electrons and holes where one must vary the effective mass and the potential. The changes in the potential function due to charge redistribution can be substantial. The charge density is non-linear in  $V(z)$ . It is linearized in each element so that the final solution may be approached iteratively starting from an initial guess for the carrier density.

The finite-difference method has been applied for Schrödinger and Poisson equation solutions. The real space along the stack has been divided into discrete uniform mesh points and equations have been solved within those discrete spacing. Then, the three-diagonal matrix has been used to extract eigenvalues and corresponding eigenvectors according to:

$$A\Psi = \lambda\Psi \quad (16)$$

where  $A$  is the three-diagonal matrix;  $\Psi$  is the eigenvector including the values  $\psi_i$  of discrete mesh and  $\lambda$  is the eigenvalue of energy. The calculated band-diagram of the p-i-n photodetectors Ge/In<sub>0.35</sub>Ga<sub>0.65</sub>As MQW heterostructure under zero bias is shown in Fig. 8. The curve gives the calculated band diagrams of the conduction and valence bands in minimums  $\Gamma$ , L and heavy hole with an absorption region consisting on 5 periods of GaAs/Ge/In<sub>0.35</sub>Ga<sub>0.65</sub>As/GaAs MQW structures optimally designed for 1.55  $\mu\text{m}$  detection. The Fermi levels are drawn with their wave functions at zero bias.

In order to identify the bias dependent dominant current components, five types of theoretical mechanisms were taken into account: diffusion currents densities ( $J_{diff}$ ), generation-recombination ( $J_{GR}$ ) currents densities, band-to-band tunneling currents densities ( $J_{BTB}$ ), TAT currents densities ( $J_{TAT}$ ) and the tunneling currents densities through the barriers ( $J_T$ ), while the conduction currents densities were reasonably neglected for this MQWs GaAs/Ge/In<sub>0.35</sub>Ga<sub>0.65</sub>As structure.  $J_{diff}$  (the diffusion current density), can be expressed as [25]

$$J_{diff} = n_i^2 \sqrt{qk_B T} \left( \frac{1}{N_A} \sqrt{\frac{\mu_e}{\tau_e}} + \frac{1}{N_D} \sqrt{\frac{\mu_h}{\tau_h}} \right) \left( e^{\frac{qV}{k_B T}} - 1 \right) \quad (18)$$

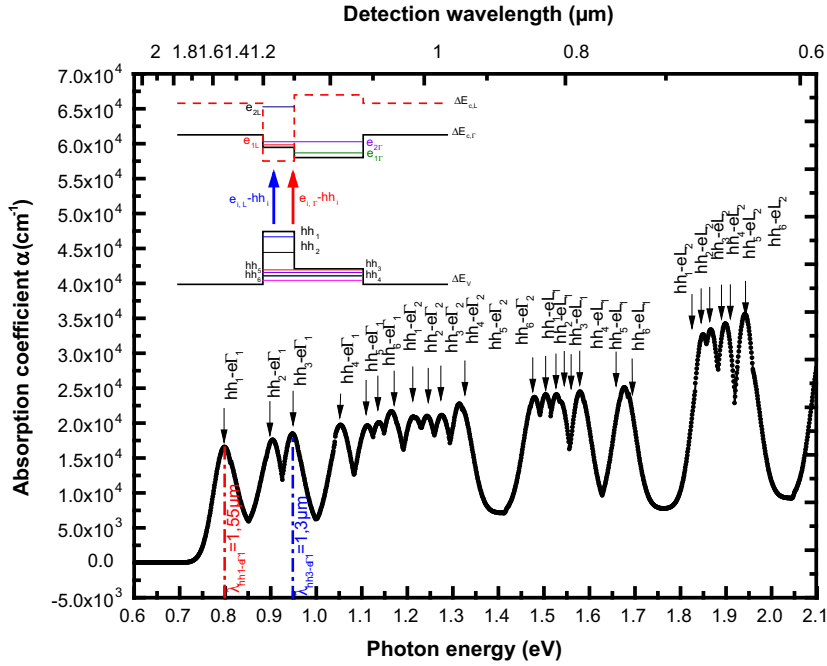


**Fig. 6.** Theoretical absorption coefficient spectra of GaAs/Ge/In<sub>0.35</sub>Ga<sub>0.65</sub>As/GaAs QW at room temperature. The peaks correspond to the hh<sub>n</sub>-eΓ<sub>m</sub> and hh<sub>n</sub>-eL<sub>m</sub> transitions ( $n = 1, 2, 3, 4, 5, 6$  and  $m = 1, 2$ ). In the inset; the conduction and valence band edge profiles, electron, hole confined states and the transitions visible in the spectra of absorption are also shown.

The wide gap of the barrier neglected the SHR generation–recombination process mainly in the valence band. For this reason,  $J_{GR}$  (the generation–recombination current density) comes only from the depletion region of the absorber and is calculated using the equation, according to the procedure outlined Ref. [26]

$$J_{GR} = \frac{qn_i}{2\tau_{GR}} \sqrt{\frac{2\epsilon_0\epsilon_r(N_A + N_D)}{qN_A N_D}} \sqrt{V_t} \left( e^{\frac{qV}{2k_B T}} - 1 \right) \quad (19)$$

The band-to-band tunneling current is from carriers that tunnel directly from the valence band on one side of the heterojunction to the conduction band located on the other side of the heterojunction. Generally, this type of current is apparent at large reverse bias because of the higher probability of band alignment. By assuming a constant built-in electric field across the depletion layer, and triangular barriers,  $J_{BTB}$  (Band to Band current density) is given by the expression [27]

$$J_{BTB} = \frac{q^3 EV \sqrt{2m_e}}{4\pi^2 \hbar \sqrt{E_g}} \exp \left( -\frac{4\sqrt{2m_e} E_g^{3/2}}{3qE\hbar} \right) \quad (20)$$

The trap-assisted tunneling current is due to carriers that occupy the trap states in the depletion region and tunnel across the junction. Transition occurs from an initially occupied energy band site to a trapping state with energy  $E$ , followed by tunneling from trap to the final energy band.  $J_{TAT}$  (Trapp assisted tunneling current density) was calculated using the following expression [28]:

$$J_{TAT} = \frac{q^2 m_T V M^2 N_t}{8\pi \hbar^3 (E_g - E_t)} \exp \left( -\frac{4\sqrt{2m_T} (E_g - E_t)^{3/2}}{3q\hbar F(V)} \right) \quad (21)$$

where  $n_i$  is the intrinsic carrier concentration in the Ge/In<sub>0.35</sub>Ga<sub>0.65</sub>As;  $q$  is the electron charge;  $k_B$  is the Boltzmann constant;  $T$  is the temperature;  $N_A$  and  $N_D$  are the  $p$ - and  $n$ -type doping concentrations, respectively;  $\mu_e$ ,  $\tau_e$  and  $\mu_h$ ,  $\tau_h$  are the mobilities and lifetimes of electrons and holes, respectively;  $\tau_{GR}$  is the generation–

combination lifetime;  $\epsilon_0$  is the permittivity of free space;  $\epsilon_r$  is the relative effective dielectric constant value of the multilayer Ge/In<sub>0.35</sub>Ga<sub>0.65</sub>As;  $V_t = V - V_d$  is the total junction potential where  $V$  is the bias voltage and  $V_d$  is the built-in potential of the heterostructure;  $F$  is the applied electric field;  $\hbar$  is the Planck constant;  $m_T$  is the reduced tunneling effective mass;  $E_g$  is the band gap;  $N_t$  is the activated trap density;  $E_t$  is the trap energy location (measured from the valence band edge); and  $M^2$  is a matrix element associated with the trap potential. The following parameters used in the simulation are summarized in Table 2.

The theoretical model used to describe the tunneling current density through the barriers, and the particle transmission through the MQW potential profile is based on the transfer matrix formalism [29,30] within the step approximation. In addition to high computational efficiency of this approach, this method is well adapted for our case. The transfer matrix  $M$  can be defined from the continuity of the wave function  $\Psi(z)$  (here  $z$  is the confinement direction) and its derivative divided by the corresponding effective mass. In our case, the energy profile  $V(z)$  is broken down into  $N + 1$  flat potential segments between two points  $z_0$  and  $z_N$  so that the solutions are plane waves:

$$\Psi(z_i) = A_i \exp(ik_i z_i) + B_i \exp(-ik_i z_i) \quad (22)$$

where  $A_i$ ,  $B_i$  and  $k_i$  are the transmitted, reflected amplitudes and the wave vector in the segment  $i$ . Hence the transfer matrix between two consecutive segments  $i$  and  $i + 1$  can be written as:

$$\frac{1}{2} \begin{bmatrix} \left(1 + \frac{m_{i+1}}{m_i} \frac{k_i}{k_{i+1}}\right) \exp i(k_i - k_{i+1})z_i & \left(1 - \frac{m_{i+1}}{m_i} \frac{k_i}{k_{i+1}}\right) \exp -i(k_i + k_{i+1})z_i \\ \left(1 - \frac{m_{i+1}}{m_i} \frac{k_i}{k_{i+1}}\right) \exp i(k_i + k_{i+1})z_i & \left(1 + \frac{m_{i+1}}{m_i} \frac{k_i}{k_{i+1}}\right) \exp -i(k_i - k_{i+1})z_i \end{bmatrix} \quad (23)$$

With this definition of the transfer matrix, one can compute the transmission coefficient for an electron with an energy  $E$  (where  $E$  is the electron longitudinal energy) to travel through  $V(z)$ . This coefficient is given by the ratio of the transmitted over incident probability currents:

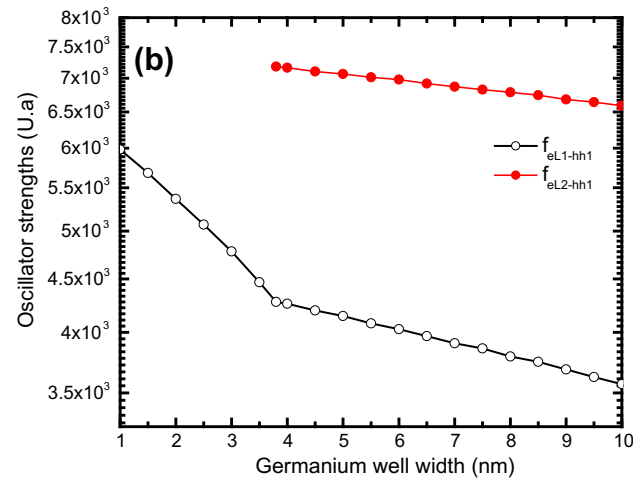
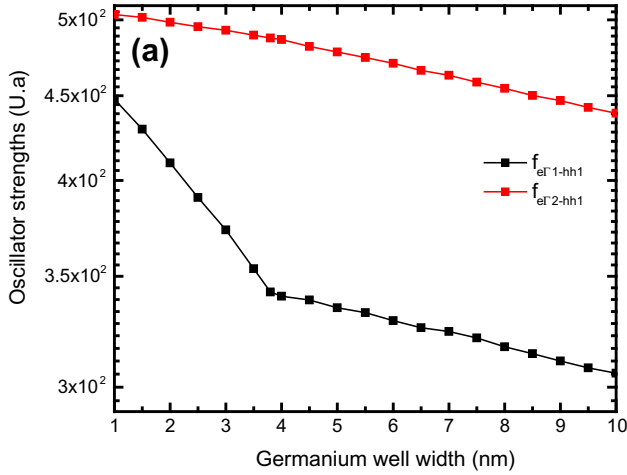


**Fig. 7.** Oscillator strength of the fundamental  $e_{c,l1}$ -hh<sub>1</sub>,  $e_{c,l2}$ -hh<sub>1</sub>,  $e_{eL,1}$ -hh<sub>1</sub> and  $e_{eL,2}$ -hh<sub>1</sub> transitions.

$$T(E) = \frac{|A_N|k_N/m_N}{|A_0|k_0/m_0} \quad (24)$$

where the indexes 0 and  $N$  correspond to the in-coming and out-going electron wave. The amplitudes  $A_N$  and  $A_0$  are related through:

$$\begin{bmatrix} A_N \\ B_N \end{bmatrix} = \prod_{i=N-1, \dots, 0} M_i \begin{bmatrix} A_0 \\ B_0 \end{bmatrix} \quad (25)$$

Following the Tsu-Esaki formalism [24] and assuming that the transverse electron energy is equal to its thermal average  $k_B T$  where  $k_B$  is the Boltzmann constant (here  $T = 300$  K), the current density will become a function of the applied bias after integration over the longitudinal energy,  $J_T$  (the tunneling current density) from extended and localized states has the form:

$$J_T = \frac{em_i^* k_B T}{2\pi^2 \hbar^3} \int_0^\infty T(E, V) \text{Ln} \left[ \frac{1 + \exp(E_f - E/k_B T)}{1 + \exp(E_f - E - eV/k_B T)} \right] dE \quad (26)$$

where  $m_i^*$  is the electrons and the heavy hole effective masse respectively,  $\hbar$  is the reduced Planck constant,  $V$  is the linear applied voltage across the active region, and the transmission coefficient  $T(E, V)$  is calculated for the specific value of  $V$ . Fig. 9(a) shows the dark current density-voltage ( $J$ - $V$ ) characteristics calculated at different temperatures ranging from 77 to 300 K on 100  $\mu\text{m}$  diameter photodetector. Excellent electrical properties were obtained, with a typical dark-current density of  $310^{-7}$  A/cm<sup>2</sup> at  $-1$  V and a differential resistance area product ( $R_0 A$ ) as good as  $3.6 \cdot 10^6 \Omega \text{ cm}^2$ . The

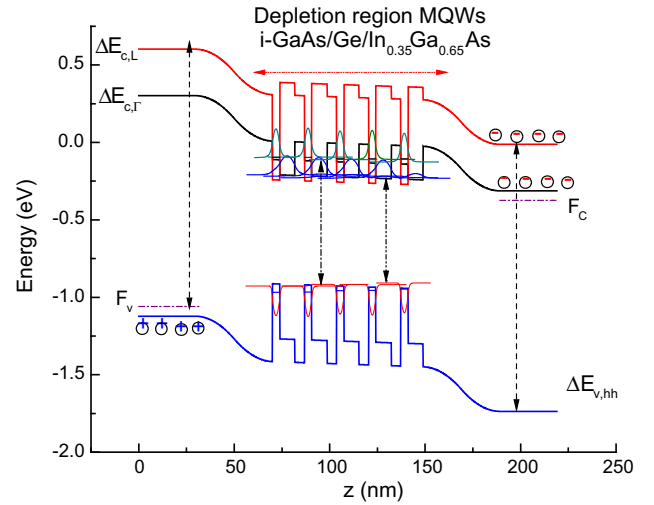


**Fig. 8.** The band-diagram of the p-i-n photodetectors Ge/In<sub>0.35</sub>Ga<sub>0.65</sub>As MQW heterostructure under zero bias.

profile of the  $R_0 A$  versus  $1000/T$  curve in Fig. 9(b) establishes that the details of modeled values to be reported elsewhere indicate that the dark current is dominated by four different mechanisms in four different temperature regimes. From 77 to 90 K, the device performance is limited by the temperature-insensitive barriers tunneling effect [31] that causes the device performance not to be good more than 90 K, the thermally generated carriers produce a stronger generation-recombination and diffusion current. From 90 to 167 K, the device is limited by the generation-recombination with an interesting recombination lifetime in the depleted region while above 110 K, the diffusion current becomes the dominant component at high temperature 167 K. In this regime, the device performance is approaching those III-V devices [32]. While in the higher temperature range (170–300 K), indicating that the dominant dark current mechanism is the thermal recombination current. The differential-resistance-area-product at zero bias as a function of  $1000/T$  for MQW GaAs/Ge/In<sub>0.35</sub>Ga<sub>0.65</sub>As/GaAs photodetector is depicted in Fig. 9(a). The asymmetry seen in the  $J$ - $V$  curves at lower temperatures is a result of dopant migration in the quantum wells. This phenomenon has been well documented in the literature [33,34]. We have also calculated the quantum efficiency  $\eta$  of the modeled photodetector. The quantum efficiency which is defined as the number of electron-hole pairs generated per incident photon on the surface of the band gap material. It arises from the contributions  $\eta_n$  and  $\eta_p$  of the two neutral regions and  $\eta_{dep}$  of the depletion region. This efficiency is given as a function of distance  $x$  from the surface by the following expression [35]:

$$\eta = \eta_p + \eta_{dep} + \eta_n \quad (27)$$

where

$$\eta_p = \frac{(1-R)\alpha L_n}{\alpha^2 L_n^2 - 1} \times \left[ \frac{\alpha L_n + \gamma_n - \exp(-\alpha(t-x_p)) \left[ \gamma_n \cosh\left(\frac{t-x_p}{L_n}\right) + \sinh\left(\frac{t-x_p}{L_n}\right) \right]}{\gamma_n \sinh\left(\frac{t-x_p}{L_n}\right) + \cosh\left(\frac{t-x_p}{L_n}\right)} - \alpha L_n \exp(-\alpha(t-x_p)) \right] \quad (28)$$

$$\eta_n = \frac{(1-R)\alpha L_p \exp(-\alpha(t+x_n))}{\alpha^2 L_p^2 - 1} \times \left[ \frac{(\gamma_p - \alpha L_p) \exp(-\alpha(d-x_n)) - \left[ \gamma_p \cosh\left(\frac{d-x_n}{L_p}\right) + \sinh\left(\frac{d-x_n}{L_p}\right) \right]}{\gamma_p \sinh\left(\frac{d-x_n}{L_p}\right) + \cosh\left(\frac{d-x_n}{L_p}\right)} + \alpha L_p \right] \quad (29)$$

**Table 2**

Material parameters used in the calculation of dark current density. All symbols have their conventional meanings.

$n_i$	$N_A$	$N_D$	$\mu_n$	$\mu_p$	$\tau_n$	$\tau_p$	$\tau_{G-R}$	$E_t$	$N_t$	$M^2$
$8.45 \times 10^8 \text{ cm}^{-3}$	$1 \times 10^{18} \text{ cm}^{-3}$	$1 \times 10^{18} \text{ cm}^{-3}$	$1100 \text{ cm}^2/\text{V s}$	$100 \text{ cm}^2/\text{V s}$	$1 \times 10^{-9} \text{ s}$	$1 \times 10^{-9} \text{ s}$	$9 \times 10^{-9} \text{ s}$	128 meV	$2 \times 10^{11} \text{ cm}^{-3}$	$1 \times 10^{-23} \text{ eV}^2 \text{ cm}^3$

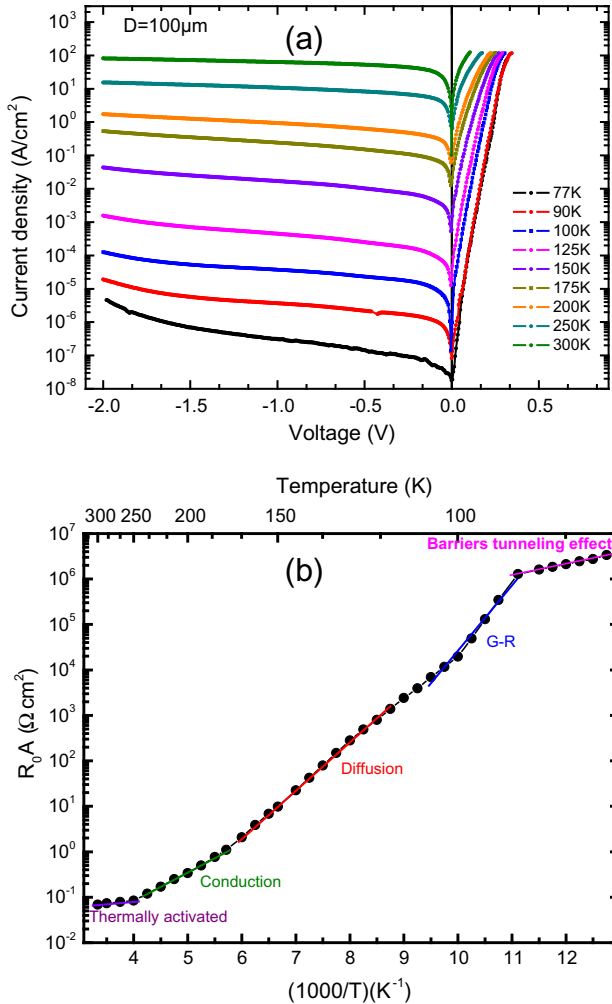


**Fig. 9.** (a) Dark current density of p-i-n heterojunction based on GaAs/Ge/In<sub>0.35</sub>Ga<sub>0.65</sub>As/GaAs MQW structures of 100 μm in diameter versus bias voltage for temperatures from 77 to 300 K. (b) Dynamic resistance-area product  $R_0A$  as a function of temperature.

$$\eta_{dep} = (1 - R) \{ \exp(-\alpha(t - x_p)) - \exp(-\alpha(t + x_n)) \} \quad (30)$$

In the above expressions:  $\gamma_n = \frac{S_n L_n}{D_n}$ ,  $\gamma_p = \frac{S_p L_p}{D_p}$ ,  $R = \frac{(n_2 - n_1)^2}{(n_2 + n_1)^2}$ ,  $L_n = \sqrt{D_n \tau_n} = \sqrt{\frac{kT}{q} \mu_n \tau_n}$  and  $L_p = \sqrt{D_p \tau_p} = \sqrt{\frac{kT}{q} \mu_p \tau_p}$  where  $\gamma_n$  and  $\gamma_p$  are the ratio of surface to bulk recombination velocity in  $p$  and  $n$  regions respectively,  $L_n$  and  $L_p$  are the electron and the hole diffusion lengths ratios in  $p$  and  $n$  regions respectively,  $S_n$  and  $S_p$  are the recombination velocities in  $p$  and  $n$  regions respectively and  $n_1$  and  $n_2$  are the refractive index of GaAs and Ge respectively [36,37].

The  $\eta$  variation with the operating wavelength of incident optical power in infrared region is shown in Fig. 10(a). The peak values of quantum efficiency occur at 1.3 and 1.55 μm are 0.78 and 0.9 respectively. The high quantum efficiency of the proposed photodetector is expected to make it an attractive choice for

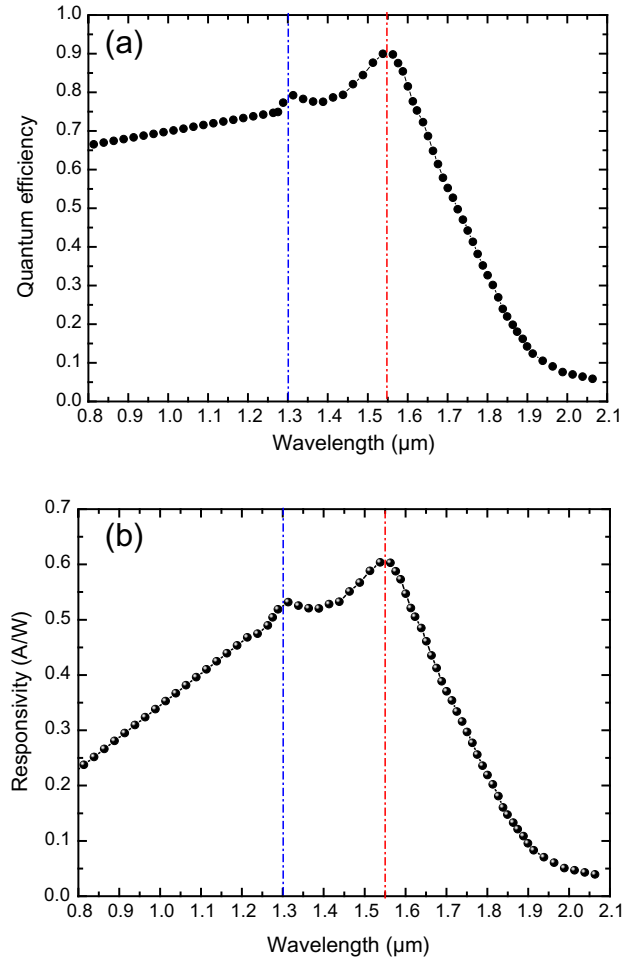


**Fig. 10.** Wavelength dependence of (a) quantum efficiency and (b) responsivity of the GaAs/Ge/In<sub>0.35</sub>Ga<sub>0.65</sub>As multi-quantum wells p-i-n photodetectors.

fabrication. Typical responsivity characteristics obtained for modeled structure is shown in Fig. 10(b). The responsivity exhibits two peaks of 0.52 A/W and 0.6 A/W at 1.3 and 1.55 μm, respectively. The GaAs/Ge/In<sub>0.35</sub>Ga<sub>0.65</sub>As superlattice p-i-n photodetectors are finding extensive applications in long haul and high bit rate optical communication systems and in local area networks for operation in the infrared region (1.3–1.55 μm) [33]. In addition to optical communication, these devices are also useful for sensing applications as they have superior electro-optical characteristics, namely low dark current, high quantum efficiency, greater sensitivity and high speed of response.

## 5. Conclusion

In conclusion, we have theoretically studied an interband infrared photodetector based on GaAs/Ge/In<sub>0.35</sub>Ga<sub>0.65</sub>As MQW heterostructure. Our investigation predicts, at room temperature, an indirect band gap for strained Ge/In<sub>x</sub>Ga<sub>1-x</sub>As semiconductor heterostructures at an In-fraction higher than 2.5% and 5%

respectively at  $\Gamma$  and L points. The active region has a quantum wells structure formed by Ge/In<sub>0.35</sub>Ga<sub>0.65</sub>As embedded in relaxed GaAs layer. The absorption spectra as well as the detection energies dependency on the Ge width have been investigated at room temperature. We explored some important properties of Ge/In<sub>x</sub>Ga<sub>1-x</sub>As heterointerface useful for optoelectronic applications. The performances of the designed photodetector operating at room temperature have been carried out using numerical simulation. It has shown five distinct regimes with different dominant mechanisms, the diffusion current density, recombination current density, the trap-assisted tunneling current density, and tunneling band-to-band current density, and the tunneling current density through the barriers. Zero-bias resistance area product of the photodetector is calculated and found to be limited by five distinct regimes. For a GaAs/Ge/In<sub>0.35</sub>Ga<sub>0.65</sub>As/GaAs based photodetector, with a thin active layer and 1.55  $\mu\text{m}$  cut off wavelength, 90% quantum efficiency and responsivity 0.6 A/W have been achieved at 300 K. These results demonstrate the importance of the selected GaAs/Ge/In<sub>0.35</sub>Ga<sub>0.65</sub>As MQW heterostructure to improve performances of infrared photodetector.

## References

- [1] F. Capasso, *Science* 235 (1987) 172.
- [2] M. Behet, R. Hovel, A. Kohl, A. Mesquida Kusters, B. Optitz, K. Heime, *Microelectron. J.* 27 (1996) 297.
- [3] W.E. McMohon, J.M. Olson, *Phys. Rev.* 60 (1999) 2480.
- [4] G. Wang, N.D. Nguyen, M.R. Leys, R. Loo, G. Brammertz, O. Richard, H. Bender, J. Dekoster, M. Meuris, M.M. Heyns, M. Caymax, *ECS Trans.* 27 (2010) 959.
- [5] W.A. Harrison, E.A. Kraut, J.R. Waldrop, R.W. Grant, *Phys. Rev. B* 18 (1978) 4402.
- [6] H. Kroemer, *J. Cryst. Growth* 81 (1987) 193.
- [7] G. Brammertz, Y. Mols, S. Degroote, V. Motsnyi, M. Leys, G. Borghs, M. Caymax, *J. Appl. Phys.* 99 (2006) 093514.
- [8] C.K. Chia, J.R. Dong, D.Z. Chi, A. Sridhara, A.S.W. Wong, M. Suryana, G.K. Dalapati, S.J. Chua, S.J. Lee, *Appl. Phys. Lett.* 92 (2008) 141905.
- [9] Yijie Huo, Hai Lin, Robert Chen, Maria Makarova, Yiwen Rong, Mingyang Li, Theodore I. Kamins, Jelena Vuckovic, James S. Harris, *Appl. Phys. Lett.* 98 (2011) 011111.
- [10] D. Haramé, J. Boquet, M. Ostling, Y. Yee Chia, G. Masini, M. Caymax, T. Krishnamohan, B. Tillack, S. Bedell, S. Miyazaki, A. Reznicek, S. Koester, *Mater. Process., Devices* 33 (6) (2010) 934.
- [11] A. Freundlich, A. Alemu, *Phys. Status Solidi C* 2 (2005) 2978.
- [12] C.K. Chia, G.K. Dalapati, Y. Chai, S.L. Lu, W. He, J.R. Dong, D.H.L. Seng, H.K. Hui, A.S.W. Wong, A.J.Y. Lau, Y.B. Cheng, D.Z. Chi, Z. Zhu, Y.C. Yeo, Z. Xu, S.F. Yoon, *J. Appl. Phys.* 109 (2011) 066106.
- [13] J. Liu, X. Sun, L.C. Kimerling, J. Michel, *Opt. Lett.* 34 (2009) 1738.
- [14] G. Bastard, *Wave Mechanics Applied to Semiconductor Heterostructures*, Halsted, New York, 1988.
- [15] N. Yahyaoui, N. Sfina, J.-L. Lazzari, A. Bournel, M. Said, *Eur. Phys. J. B* 86 (2013) 259.
- [16] N. Yahyaoui, N. Sfina, J.-L. Lazzari, A. Bournel, M. Said, *J. Appl. Phys.* 115 (2014) 033109.
- [17] Yu Bai, Kenneth E. Lee, Chengwei Cheng, Minjoo L. Lee, Eugene A. Fitzgerald, *J. Appl. Phys.* 104 (2008) 084518.
- [18] M. Yamanishi, I. Suemune, *Jpn. J. Appl. Phys.* 23 (1984) 35.
- [19] B.N. Zvonkov, A.A. Biryukov, A.V. Ershov, S.M. Nekorkin, V.Ya. Aleshkin, V.I. Gavrilenko, A.A. Dubinov, K.V. Maremyanin, S.V. Morozov, A.A. Belyanin, V. Kocharovskiy, V.I.V. Kocharovskiy, *Appl. Phys. Lett.* 92 (2008) 021122.
- [20] G.-E. Chang, S.-W. Chang, S.L. Chuang, *IEEE J. Quantum Electron.* 46 (2010) 1813.
- [21] W.Q. Chen, T.G. Andersson, *J. Appl. Phys.* 73 (1993) 4484.
- [22] F. Ben Zid, A. Bouri, H. Mejri, R. Tlili, M. Said, F.A. D'Avitaya, J. Derrien, *J. Appl. Phys.* 91 (2002) 9170.
- [23] J.A. Berashevich, A.L. Danilyuk, A.N. Kholod, V.E. Borisenko, *Mater. Sci. Eng., B* 101 (2003) 111.
- [24] I.-H. Tan, G.L. Snider, L.D. Chang, E.L. Hu, *J. Appl. Phys.* 68 (1990) 4071.
- [25] V. Gopal, E. Plis, J.B. Rodriguez, C.E. Jones, L. Faraone, S. Krishna, *J. Appl. Phys.* 104 (2008) 124506.
- [26] A. Jdidi, N. Sfina, S. Abdi-Ben Nassrallah, M. Saïd, J.L. Lazzari, *Semicond. Sci. Technol.* 26 (2011) 125019.
- [27] S.M. Sze, *Physics of Semiconductor Devices*, second ed., Wiley, New York, 1981.
- [28] Q.K. Yang, F. Fuchs, J. Schmitz, W. Pletschen, *Appl. Phys. Lett.* 81 (2002) 4757.
- [29] N. Yahyaoui, N. Sfina, S. Abdi-Ben Nasrallah, J.-L. Lazzari, M. Said, *Comput. Phys. Commun.* 185 (2014) 3119.
- [30] E. Larkins, C.H. Schneider, S. Ehret, J. Fleibner, B. Dischler, P. Koidl, J.D. Ralston, *IEEE Trans. Electron Devices* 41 (1994) 511.
- [31] D. Ahn, S.L. Chuang, *IEEE J. Quantum Electron.* 23 (1987) 2196.
- [32] X. Han, J. Li, J. Wu, G. Cong, X. Liu, Q. Zhu, Z. Wang, *Physica E* 28 (2005) 230.
- [33] H.C. Liu, Z.R. Wasilewski, M. Buchanan, H. Chu, *Appl. Phys. Lett.* 63 (1993) 761.
- [34] Z.R. Wasilewski, H. C Liu, M. Buchanan, *J. Vac. Sci. Technol., B* 12 (1994) 1273.
- [35] P. Chakrabarti, A. Gawarikar, V. Mehta, D. Garg, *J. Microwaves Optoelectron.* 5 (1) (2006).
- [36] D.T.F. Marple, *J. Appl. Phys.* 35 (1964) 1241.
- [37] D.E. Aspnes, A.A. Studna, *Phys. Rev. B* 27 (1983) 985.